optica

Ultralow transmission loss in inhibited-coupling guiding hollow fibers

B. Debord,[1,2,5] A. Amsanpally,[1] M. Chafer,[1,2] A. Baz,[1] M. Maurel,[1,2] J. M. Blondy,[1] E. Hugonnot,[3] F. Scol,[3] L. Vincetti,[4] F. Gérôme,[1,2] and F. Benabid[1,2,*]

[1]GPPMM Group, Xlim Research Institute, CNRS UMR 7252, University of Limoges, Limoges, France
[2]GLOphotonics S.A.S, 1 avenue d'Ester, Ester Technopôle, Limoges, France
[3]Commissariat à l'Energie Atomique et aux Energies Alternatives, Centre d'Etudes Scientifiques et Techniques d'Aquitaine, 33116 Le Barp Cedex, France
[4]Department of Engineering "Enzo Ferrari," University of Modena and Reggio Emilia, I-41125 Modena, Italy
[5]e-mail: benoit.debord@xlim.fr
*Corresponding author: f.benabid@xlim.fr

Received 21 September 2016; revised 22 December 2016; accepted 2 January 2017 (Doc. ID 275015); published 8 February 2017

Attenuation in photonic bandgap guiding hollow-core photonic crystal fiber (HC-PCF) has not beaten the fundamental silica Rayleigh scattering limit (SRSL) of conventional step-index fibers due to strong core-cladding optical overlap, surface roughness at the silica cladding struts, and the presence of interface modes. Hope has been revived recently by the introduction of hypocycloid core contour (i.e., negative curvature) in inhibited-coupling guiding HC-PCF. We report on several fibers with a hypocycloid core contour and a cladding structure made of a single ring from a tubular amorphous lattice, including one with a record transmission loss of 7.7 dB/km at ~750 nm (only a factor ~2 above the SRSL) and a second with an ultrabroad fundamental band with loss in the range of 10–20 dB/km, spanning from 600 to 1200 nm. The reduction in confinement loss makes these fibers serious contenders for light transmission below the SRSL in the UV–VIS–NIR spectral range and could find application in high-energy pulse laser beam delivery or gas-based coherent and nonlinear optics. © 2017 Optical Society of America

OCIS codes: (060.2280) Fiber design and fabrication; (060.5295) Photonic crystal fibers; (060.2270) Fiber characterization.

https://doi.org/10.1364/OPTICA.4.000209

1. INTRODUCTION

Since its first proposal [1], hollow-core photonic crystal fiber (HC-PCF) has proved to be a remarkable platform for our understanding on how light is confined in such microstructured waveguides, and an outstanding host for gas–laser applications [2,3].

In HC-PCF, a core-guided mode is prevented from coupling to the cladding by either photonic bandgap (PBG) [1] or inhibited-coupling (IC) [4]. In PBG guiding fibers, the coupling of the core mode to the cladding is disallowed by microengineering the cladding structure such that its modal spectrum is void from any propagation modes at the core guided-mode effective index-frequency space, $n_{\text{eff}} - \omega$ (i.e., $\{|\varphi_{\text{clad}}\} = \emptyset$, with φ_{clad} being the field wave function of the propagating mode in the cladding structure) [1]. The lowest transmission loss of 1.2 dB/km at 1620 nm achieved with this type of HC-PCF 12 years ago is set not by confinement loss (CL) but by surface-roughness scattering loss (SSL) [5]. The latter scales with the amount of the optical overlap of the guided light with the silica core contour (typically in the range of 1%–0.1%), and increases with wavelength shortening following $\sim\lambda^{-3}$ scaling law. Furthermore, all reported PBG HC-PCFs operating below 800 nm have transmission loss higher than 100 dB/km because of the difficulty of drawing smaller-pitch PBG HC-PCF with comparable core–surface uniformity to those operating at longer wavelengths.

For the case of IC guidance, the condition of a PBG is no longer required. In analogy with quasi-bound and bound state in a continuum (QB-BIC), first proposed by Van Neumann and Wigner in 1929 within the context of quantum mechanics [6], a core guided mode and cladding modes can have the same effective index and yet propagate without strong interaction. Though QB-BIC remains an uncommon scheme of trapping waves, it is universal, as shown in a recent review on the subject matter [7]. In the optical fiber form, QB-BIC works as follows: a core guided mode (often leaky mode) cannot, or is strongly inhibited to, channel out through the cladding by a strong reduction in the coupling between the cladding mode continuum and a core mode. In other words, the dot product between the field of the core mode $|\varphi_{\text{core}}\rangle$ and the cladding mode $|\varphi_{\text{clad}}\rangle$ is strongly reduced (i.e., $\langle\varphi_{\text{clad}}|\Delta n^2|\varphi_{\text{core}}\rangle \to 0$, with Δn being the photonic structure transverse index profile). This can be done either by having little spatial intersection between the fields of $|\varphi_{\text{clad}}\rangle$ and $|\varphi_{\text{core}}\rangle$ or by having a strong mismatch in their respective transverse spatial phases.

In a previous paper [4], the design parameters for optimal IC guidance in air–silica HC-PCF such as Kagome lattice cladding

have been laid down. It has been shown that IC guidance is enhanced by having a glass microstructure exhibiting a very thin and elongated glass–membrane network with a minimum number of sharp bends or nodes, and by operating in the large-pitch regime or high normalized frequency (i.e., the lattice pitch is larger than the optical wavelength λ) [8]. These structural features ensure modes with strong localization in the thin silica web and with a very fast transverse field oscillation (i.e., high azimuthal-like number). Furthermore, unlike with PBG, the criterion $\langle\varphi_{\text{clad}}|\Delta n^2|\varphi_{\text{core}}\rangle \to 0$ implies a CL with a strong dependence on the core-mode profile, and thus the core contour. This led to the seminal introduction of hypocycloid core-contour design (i.e., negative curvature) in 2010 [9,10], and which resulted in a dramatic reduction in transmission loss, as illustrated in the 17 dB/km at 1 μm achieved with Kagome lattice HC-PCF and its record optical power handling [11,12]. This in turn has triggered a wide effort to design hollow-core fibers with negative curvature [13,14]. In a hypocycloid core-contour fiber, the core has a contour exhibiting a set of alternating negative curvature cups with inner radius R_{in}, and a field overlap integral between the core mode and the highly oscillating silica core-surround mode (cladding mode) that is strongly reduced compared to the previous circular or hexagonal shape in Kagome HC-PCF [8]. Three reasons explain such a reduction. First, the HE_{11} mode field spatial overlap with silica at R_{in} is reduced to the tangent sections of the inner cups of the hypocycloid contour. Second, the larger perimeter of the hypocycloid contour compared to a circle with radius R_{in} results in a higher azimuthal-like number in the silica core-surround modes, and hence stronger transverse phase mismatch with the core mode. Finally, the spatial overlap between the core mode with connecting nodes—which support low azimuthal number modes—is strongly reduced [10,15,16].

These features for IC guidance are also fulfilled in a tubular lattice, which consists of an arrangement of isolated thin glass tubes [17], and its fiber form exhibits a hypocycloid core contour [13]. More crucially, when the cladding is reduced to a single ring of an aperiodic lattice of such tubes, one can fabricate a fiber with a core contour that is completely void of any connecting nodes (as proposed in [18]), which strongly favors IC [4,13]. As a matter of fact, because of the very weak HE_{11} core-mode field overlap with the cladding in IC guiding fibers, low confinement loss can be expected with only one cladding ring. This is experimentally illustrated by the results obtained with a hollow-core fiber having a single ring of this cladding amorphous lattice [13,14]. In these works, the fiber cladding tubes were relatively thick (>1 μm), and the achieved transmission loss was as low as 34 dB/km in a 3–4 μm spectral range. More recent works achieved 30 dB/km at 1 μm using tube thickness of 830 nm [19] and broad fundamental band with thinner tubes (down to thickness of 360 nm) [20].

Here, by optimizing such a tubular cladding and operating with a much thinner glass tube than has previously been achieved, we report on the fabrication of several ultralow-loss single-ring tubular lattice HC-PCFs (SR-TL HC-PCF) guiding in the UV–VIS and NIR. Among the fabricated fibers, we count one with a record transmission loss of 7.7 dB/km at ~750 nm, which is only 4 dB above the Rayleigh scattering fundamental limit in silica, and observed guidance down to 220 nm. The loss figure of 7.7 dB/km is lower than ~12 dB/km, which is the PBG projected loss at 750 nm. It is also more than one order of magnitude less than any reported PBG HC-PCF guiding below 800 nm. We count a second fiber that exhibits an ultrabroad fundamental band with loss range of 10–20 dB/km over one octave spanning from 600 to 1200 nm. Both fibers present a near single-modedness, with ~20 dB extinction between HE_{11} fundamental core mode and the strongest first higher-order mode (HOM), and exhibit bend loss of 0.03 dB/turn for a 30 cm bend diameter at 750 nm. Finally, the results indicate that the SSL is currently the limiting factor for wavelengths shorter than 1 μm.

2. FIBER PARAMETER DESIGN

The left panel of Fig. 1(a) shows an example of the SR-TL HC-PCF that we are exploring. To understand and determine the design parameters for fiber optimal guidance, we first examine the nature of its cladding modes. For this purpose, one can consider the SR-TL HC-PCF as an air defect (i.e., core) surrounded by one ring of an amorphous lattice of isolated tubes (i.e., cladding) [21,22]. In order to calculate the modal spectrum of such an amorphous lattice, we exploit the fact that we operate in the large pitch regime [8,23]. Under this regime, the photonic structure is primarily governed by the modal properties of the lattice single unit rather than their arrangement in the lattice [23]. Consequently, the modal spectrum of the SR-TL HC-PCF cladding can be determined by considering an infinite lattice of any symmetry arrangement [see Supplement 1 for the numerical corroboration (Section 1) and its entailed physical background (Section 2)]. Here, we take a triangular arrangement to calculate the modal spectrum of the SR-TL HC-PCF cladding [see central and right panels of Fig. 1(a)].

Figure 1(b) maps the photonic structure propagation modes in the space $n_{\text{eff}} - F$ for a lattice of isolated glass tubes of refractive index $n_g = 1.45$ and with representative radius $R_t = 7$ μm, thickness $t = 400$ nm, and gap between two adjacent tubes $\delta = 4$ μm (corresponding to a lattice pitch of 18 μm, which is much larger than any of our operating wavelengths). Here, $F = (2t/\lambda)\sqrt{n_g^2 - 1}$ is a normalized frequency relative to the tube thickness and refractive index of the glass and air. The plot shows the density of photonic states (DOPS) normalized to that of the vacuum [24] (see Supplement 1 for calculation details). The DOPS diagram shows no PBG regions in the mapped $n_{\text{eff}} - F$ space, but a quasi-continuum of propagating modes. The nature of these modes is revealed in Fig. 1(c) by showing the transverse profile of their field magnitude for two frequencies ($F = 0.8$ and $F = 1.2$) at two representative sets of n_{eff}. Within the first set [from 1.2 to 1.3; see the shaded light-red rectangle of Fig. 1(c)], the modes are all located in the silica tube as expected and are identifiable in the DOPS diagram by their steep dispersion curves (close to vertical). The second set of n_{eff} crosses the vacuum-line (i.e., $n_{\text{eff}} = 1$) and ranges from 1.04 to 0.99 [see the dotted blue rectangle of Fig. 1(c)]. Within this n_{eff} range, the modal content exhibits, in addition to the just-discussed silica modes, modes residing in air having flat dispersion curves (close to horizontal). Furthermore, and except for $F \approx 1$, air-residing modes seem to have little interaction with the silica modes as shown by the distinguishable profile of their dispersion curves. This is in contrast with the strong hybridization between the air and silica modes at $F \approx 1$ as shown by the "anti-crossing shape" in the DOPS. This DOPS modal spectral structure, and especially the non-hybridization of modes from two different materials like air and silica, can be explained by considering the transverse wave

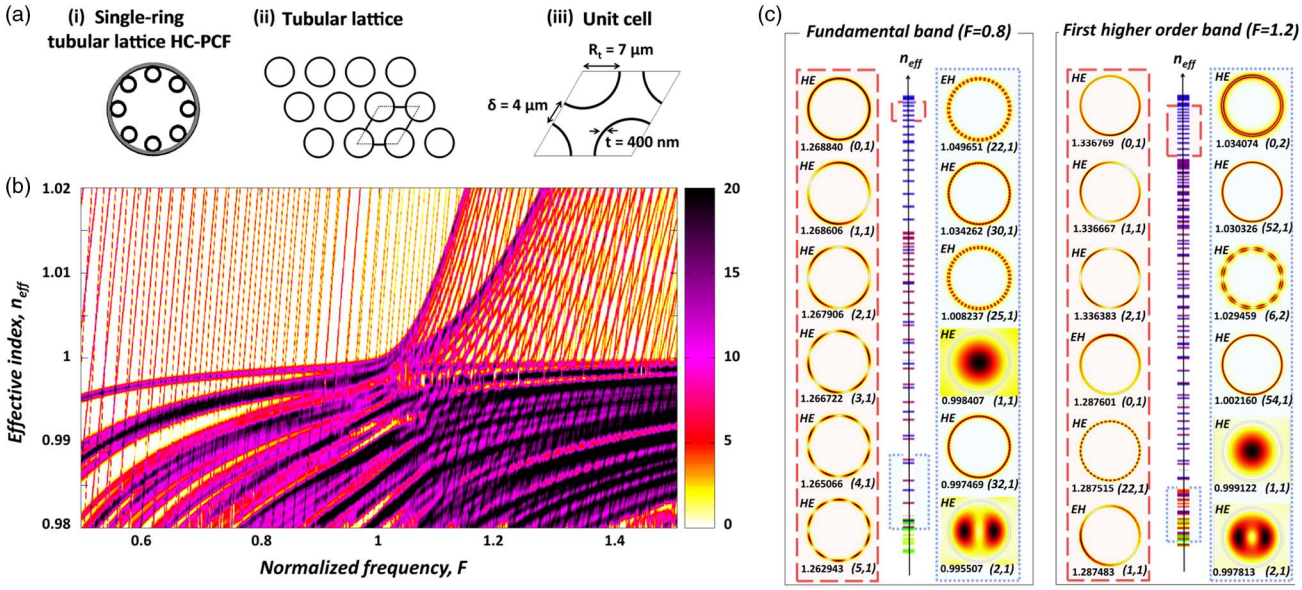

Fig. 1. (a) Schematic of HC-PCF with a single-ring tubular amorphous lattice (i), section of a tubular lattice in a triangular arrangement (ii), and the details of its unit cell (iii). δ is the inter-tube gap distance, R_t is the tube radius, and t is the tube ring thickness. (b) Density of photonic state (DOPS) of an infinite tubular lattice in triangular arrangement. The DOPS value is normalized to that of the vacuum. (c) Transverse profiles of the electric field magnitude of the photonic state (modes) for $F = 0.8$ (fundamental band) and $F = 1.2$ (first higher-order band). The vertical axes are the lattice mode effective indices at $F = 0.8$ and $F = 1.2$. The displayed profiles correspond to modes with effective index above (dashed red box) and crossing (dotted blue box) the vacuum line. The label on the top left of the mode profile corresponds to the nature of the mode (HE or EH). The numbers at the bottom of the mode profile correspond, respectively, to the mode effective index and to the indices of the azimuthal and radial components of the transverse wave number, respectively (m, l).

vector components of each mode. Here, the field profile and dispersion of each mode far from an anti-crossing region can be approximated to HE_{ml} (i.e., electric field direction is azimuthal) or EH_{ml} (i.e., electric field direction is radial) given in [25] for the silica modes, and to those given by Marcatili and Schmeltzer for the air modes [26]. The suffixes m and l are the indices of the azimuthal and radial components of the transverse wavenumber, respectively. When the silica modes are longitudinally phase-matched with an air mode (i.e., they have equal n_{eff}), and considering our case of wavelength much smaller than the radius of the tube, m and l are related via the following identity (see Supplement 1, Section 2):

$$\left(\frac{m}{2R_t}\right)^2 + \left((l-1)\frac{\pi}{t}\right)^2 \approx (2\pi/\lambda)^2(n_g^2 - 1). \quad \textbf{(1)}$$

Furthermore, the silica and air modes strongly hybridize when they are also transversely phase-matched. For the case of low-azimuthal-number air mode such as HE_{11}, this occurs when the silica mode azimuthal number is nil or close to zero [17]. This means that the radial number takes the identity $(l-1)(\pi/t) \approx (2\pi/\lambda)\sqrt{n_g^2 - 1}$ or $F \approx (l-1)$ (see Supplement 1, Section 2). As shown in the DOPS diagram near the vacuum line, the just-shown relations split the lattice modal spectrum into radial number indexed bands located between $F \approx (l-1)$ and $F \approx l$. Each band is populated by silica modes characterized with a fixed l and azimuthal number given by Eq. (1). These transverse wavenumber indices are also defining parameters for the transmission spectral structure and confinement loss of a HC-PCF whose cladding is made up of such a tubular amorphous lattice. Indeed, Eq. (1) and the transverse phase-matching condition hold for the fiber air core modes in the same manner as with those of the cladding tube. Consequently, the fiber transmission will exhibit band edges at $F \approx l$, corresponding to phase matching with cladding modes having m nil or close to zero. This transverse phase-matching condition can be written in the form $\lambda_{l-1} = (2t/(l-1))\sqrt{n_g^2 - 1}$, which is used in some of the current literature as a defining feature of fibers guiding via anti-resonance reflecting optical waveguide (ARROW) [23,27]. In Supplement 1 (Section 3), we provide some distinctive properties to differentiate between PBG, IC, and ARROW, and discuss why the latter is not appropriate in comprehensibly describing the guidance in fibers such as SR-TL HC-PCF. Conversely, in each band, the fiber confinement loss α_{CL} is set by the quantity $\langle\varphi_{\text{clad}}|\Delta n^2|\varphi_{\text{core}}\rangle$, through $\alpha_{\text{CL}} \propto |\langle\varphi_{\text{clad}}|\Delta n^2|\varphi_{\text{core}}\rangle|^2$ [28], which quantifies the strength of the power coupling between the core and cladding modes [4]. Similar to coupled mode theory results [29,30], $\langle\varphi_{\text{clad}}|\Delta n^2|\varphi_{\text{core}}\rangle$ scales with the ratio between the normal modes' transverse phase mismatch and their field spatial overlap. In Supplement 1 (Section 5) we show that $\alpha_{\text{CL}} \propto \text{DO}/g(m)$ for the fiber-core HE_{11}, with DO being the optical overlap of HE_{11} with the cladding silica dielectric and $g(m)$ being a positive and increasing function of m.

Furthermore, from Eq. (1), it is easy to note that increasing m can be achieved by either increasing the silica tube radius or increasing t/λ, which is consistent with the results reported in [9,10,31]. However, because R_t is interconnected with the fiber core radius R_c, δ, and the number of tubes in the cladding ring N through the identity $R_t = (R_c \sin(\pi/N) - \delta/2)(1 - \sin(\pi/N))^{-1}$, its increase can have reverse impact on both the fiber CL and modal content. In order to find the best

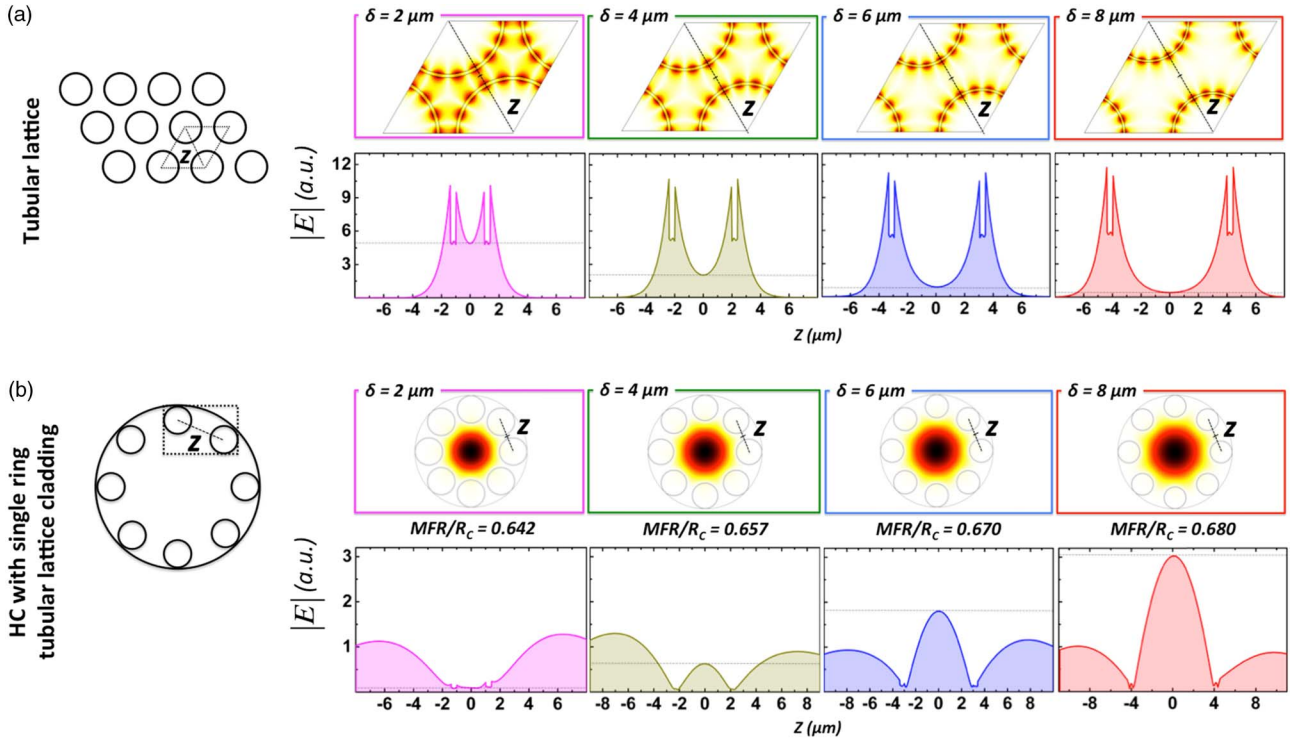

Fig. 2. (a) Field amplitude transverse profile of a unit cell of tubular lattice (top left). First row shows its evolution with inter-tube gap δ when varied from 2 to 8 μm, and second row shows 1D profile along the gap line (labeled "z") between the center of two adjacent tubes. (b) Field amplitude transverse profile of a fiber core with tubular amorphous lattice cladding (bottom right schematics) and its evolution with δ (third row). MFR/RC is the ratio between the mode-field radius (MFR) and the fiber core inner radius R_c. 1D profile of the fiber core mode along a cladding inter-tube line (labeled "z"). Here, the wavelength of the modes is 700 nm.

tradeoff between these parameters, we start by finding out the optimal δ, then the number N, and finally the fiber core radius.

Figure 2(a) illustrates the effect of increasing δ on the cladding modal spectrum by the evolution of the electric field magnitude of a representative silica mode [$EH_{9,2}$ at wavelength of 700 nm for $t = 400$ nm (i.e., $F = 1.2$) and tube radius of $R_t = 7$ μm]. The results show that increasing δ from 2 to 8 μm results in a decrease of the mode n_{eff} from ∼1.00062 to 0.99993 and stronger light confinement in the silica tube, as shown in the 1D profile along a gap line joining the center of two adjacent tubes [z line in Fig. 2(a), bottom panel]. This trend favors larger inter-tube gap for IC; however, this would make sense only if the fiber core mode profile is not altered and kept its zero-order Bessel profile. Figure 2(b) shows the evolution of the HE_{11} core mode of a single-ring tube lattice fiber with eight tubes when the gap is increased. The results show that increasing δ from 2 to 8 μm leads to an increase of the mode-field radius relative to the fiber core radius R_c by almost 6%, which entails a stronger optical spatial overlap of the mode with the silica. The bottom panel of Fig. 2(b) clearly shows the increase with δ of field magnitude along the gap line, indicative of the stronger spread of the core mode in the cladding. Equally, we investigated the effect of δ on the core mode leakage by calculating the power flux along the fiber radial and transverse directions using the Poynting vector (see Supplement 1, Section 4). The results clearly demonstrate that the transverse power leakage of the HE_{11} core mode at the gaps strongly increases with increasing δ, and enhances by up to 30 dB when δ is increased from 2 to 8 μm for $\lambda = 530$ nm. The results also show that the primary power leakage channels are the touching nodes between the tube and the outer silica jacket for $\delta < 4$ μm, and the inter-tube gap for $\delta > 6$ μm. Consequently, and given the stronger impact of the core radius on the confinement loss ($\alpha_{\text{CL}} \propto R_c^{-4}$[31]) compared to that induced by the observed cladding modal change, the optimal δ will be a tradeoff between a value that is sufficiently small to avoid a core mode leakage being too high, and sufficiently large to avoid a coupling between the tubes being too strong or the formation of connecting nodes (which support low-azimuthal-number modes) during the fabrication process.

The top of Fig. 3 summarizes the effect of N and δ on the fiber confinement loss. Figure 3(a) shows the CL over a representative spectrum for different N and for fibers with fixed $t = 400$ nm, $R_t = 8$ μm, and $\delta = 5$ μm. The loss is expressed as $\alpha_{\text{CL}} R_c^4$ so as to only keep the effect of N on the transmission loss trend with increasing N independent from the associated fiber core radius change. The results show that, for the same core radius, the CL decreases with increasing N. However, the decrease rate of the CL with N drops as N gets larger. For example, choosing a wavelength of 540 nm, $\alpha_{\text{CL}} R_c^4$ decreases by a factor of 3 when N is changed from 5 to 6. However, it decreases by less than 20% when the tube number is increased from 8 to 9. This is due to the resonance between the core mode and the air modes of the tubes [15,17]. On the other hand, the power ratio of the higher-order core modes TE_{01} and HE_{11}, which is an indicator of how well the fiber can operate in a single-mode manner, increases with decreasing N, thus favoring a smaller number of tubes for single-mode operation [see Fig. 3(b)]. Consequently, the optimal N is the result of a tradeoff between CL decrease, which scales

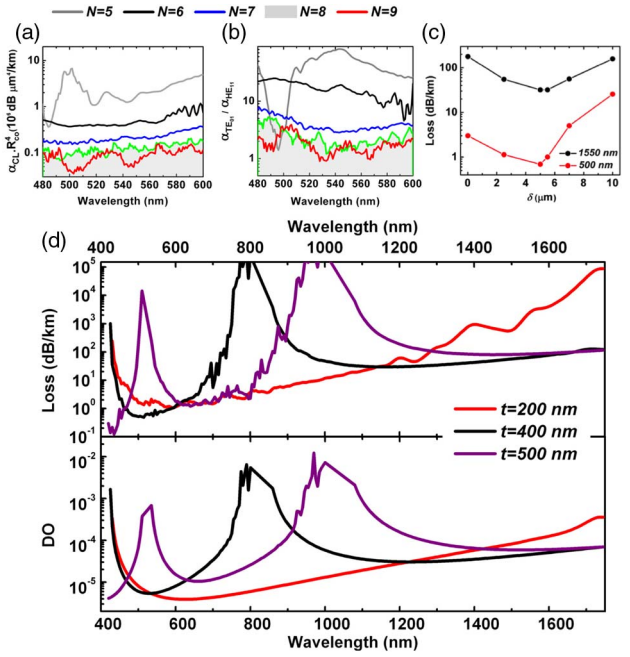

Fig. 3. (a) CL for different N. (b) Ratio between TE_{01} and HE_{11} loss. (c) Loss spectra versus δ. (d) Loss and optical overlap of HE_{11} with the cladding silica dielectric (DO) spectra for different t values (200, 400, and 500 nm).

proportionally with N; the fiber single-modedness, which is inversely proportional to N; and bend loss sensitivity, which favors smaller fiber core size and thus smaller N. We found $N = 8$ to be a good compromise for a sufficiently low CL and a modal content dominated by the HE_{11} mode. Figure 3(c) shows the CL evolution with δ at two representative wavelengths of a SR-TL HC-PCF with $N = 8$, $t = 400$ nm, and $R_t = 8$ μm. The results show that the inter-tube gap range of 2–6 μm is suitable for low-loss guidance. Based on these design results, we calculated the CL spectra for different tube thicknesses. Figure 3(d) shows the spectra of CL (top) and DO (bottom) at different tube thicknesses ($t = 200$, 400, and 500 nm) for a SR-TL HC-PCF with $N = 8$, $R_t = 8$ μm, and $\delta = 2.5$ μm. Within the explored wavelength range of 400–1750 nm, the $t = 200$ nm fiber exhibits one large transmission band corresponding to the fundamental band with a minimum loss of ~1 dB/km at wavelengths near 600 nm. For the $t = 400$ nm SR-TL HC-PCF, the spectrum exhibits two transmission bands separated by a high-loss band centered around 800 nm. Here, the lowest-loss figure is 0.5 dB/km and occurs at wavelengths near 500 nm in the first higher-order transmission band. For $t = 500$ nm SR-TL HC-PCF, we observe a spectrum with the three transmission bands and lowest loss of 0.3 dB/km occurring in the second higher-order band around 480 nm. Below, we explore these results and scaling laws in the fabrication of several fibers with $N = 8$. The DO spectra show the same resonance structure as CL as expected by IC guidance, and values in the range of 10^{-5}–10^{-6}. The minimum obtainable loss can be reduced by further thinning the tube thickness and operating in the shorter wavelength as the silica cladding modes get more localized with F increase.

Finally, the consistency of the observed CL slope with wavelength between fibers with different t and the scaling law $m \propto 1/t$ is noteworthy (see Supplement 1, Section 6).

3. EXPERIMENTAL RESULTS

Figure 4(a) shows the micrographs of four fabricated SR-TL HC-PCFs along with their physical properties. The experimental fibers have been fabricated using the stack-and-draw technique. Here, we endeavored to vary δ while keeping R_t, t, and R_c as constant as possible so as to find out the optimal value from the standpoint of fabrication and transmission performance. The table summarizing these values for the different fibers shows that δ spans from 2.7 μm (Fiber #4, pink-colored micrograph frame) to 8 μm (Fiber #1, green-colored micrograph frame). Within this δ span, the core radius R_c ranges from 13.75 to 18.5 μm, corresponding to a maximum relative difference between the different fiber core sizes of less than 35%. Similarly, the cladding tube radius R_t and t range from 5.1 μm to 6.15 μm and from 415 nm to 580 nm, respectively, with a maximum relative difference less than 20% and 40%, respectively. Figure 4(b) shows the four fibers' measured loss spectra versus λ/t. As expected, for the measured wavelength range of 400–1750 nm and tube thickness of 415–580 nm, the spectra show three transmission bands corresponding to the fundamental band ($\lambda/t > 2$), first-order band ($1 < \lambda/t < 2$), and second-order band ($\lambda/t < 1$). The different fiber-loss curves in the fundamental and first-order bands clearly demonstrate a dramatic reduction

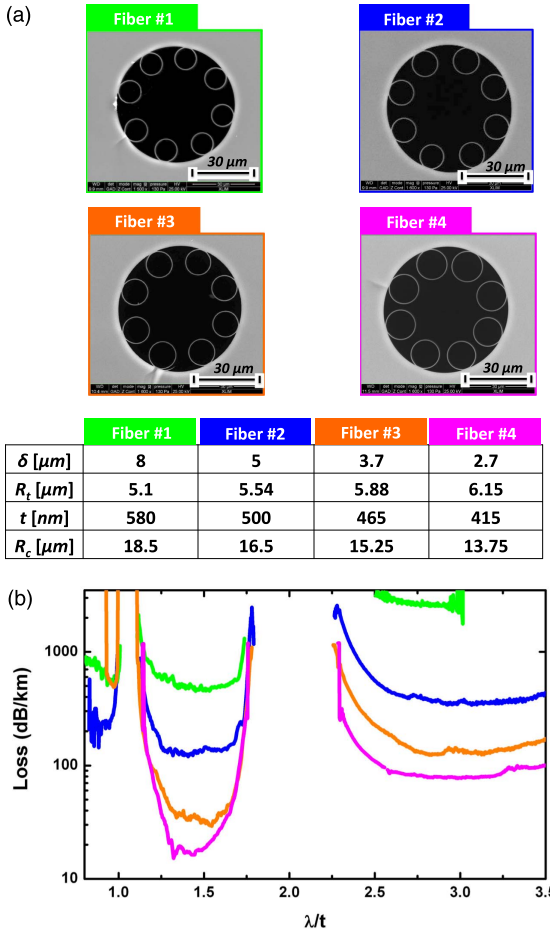

	Fiber #1	Fiber #2	Fiber #3	Fiber #4
δ [μm]	8	5	3.7	2.7
R_t [μm]	5.1	5.54	5.88	6.15
t [nm]	580	500	465	415
R_c [μm]	18.5	16.5	15.25	13.75

Fig. 4. (a) SEM pictures of four fabricated HC tubular lattice fibers with corresponding geometrical parameters (δ, R_t, t, R_c). (b) Experimental evolution of the loss spectrum with the gap between the tubes.

of the optical attenuation with δ decrease, from near 1 dB/m loss level for $\delta = 8$ μm (green curve) down to only a few tens of dB/km for $\delta = 2.7$ μm.

For the second-order band, the trend of the loss decrease with δ is observed only for δ range of 5–8 μm. For smaller inter-tube gaps corresponding to tube thicknesses t smaller than 500 nm, the loss increases with δ decrease (e.g., orange curve compared to the blue curve). Furthermore, a comparison of the rate at which the loss decreases with the gap shortening shows that the loss in the fundamental band decreases at a larger rate than that in the first-order band. As a matter of fact, it plateaus down to 15 dB/km for δ range of 3.7–2.7 μm (see pink and orange curves). Finally, because the attenuation due to the surface roughness scattering is not taken into account in the calculated CL, the measured loss spectra don't necessarily decrease with decreasing wavelength. This scattering loss stems from the fiber core surface roughness due to frozen capillary waves during the fiber draw [5] and takes the form of $\alpha_{SSL}(\lambda) = \varsigma \cdot F_{cc}(\lambda) \cdot \lambda^{-3}$ [5,32], with ς being a constant related to the surface roughness root-mean-square height and $F_{cc}(\lambda)$ being the core mode overlap with the core contour. In the case of IC guiding HC-PCF, the confinement loss dependence on the core mode overlap with the cladding raises the question of whether the surface roughness affects the CL. In order to address this question, we considered the simulation of several SR-TL HC-PCFs with their tubes exhibiting corrugated surfaces to mimic a surface roughness along the azimuthal direction (see Supplement 1, Section 7 for more details). The results show that CL changes little for wavelengths larger than 800 nm but increases for shorter wavelengths, consistent with the observed higher transmission loss at short wavelengths in the early IC guiding hypocycloid core-contour HC-PCF [9–11,15,33].

Now that δ value impact on the transmission loss of fabricated fibers is demonstrated, we use $\delta \sim 2.5$ μm as a parameter target and undertake two fiber-fabrication campaigns with different aims. The first aim consists of the fabrication of fibers with the thinnest tubes possible so as to have the broadest fundamental band while having loss figures as low as the surface-roughness-induced transmission loss could permit. The second aim is to have the lowest loss figure possible in the NIR–VIS spectral range. This was undertaken in an iterative process of several fiber draws. As mentioned previously, having a too-thin cladding tube (typically

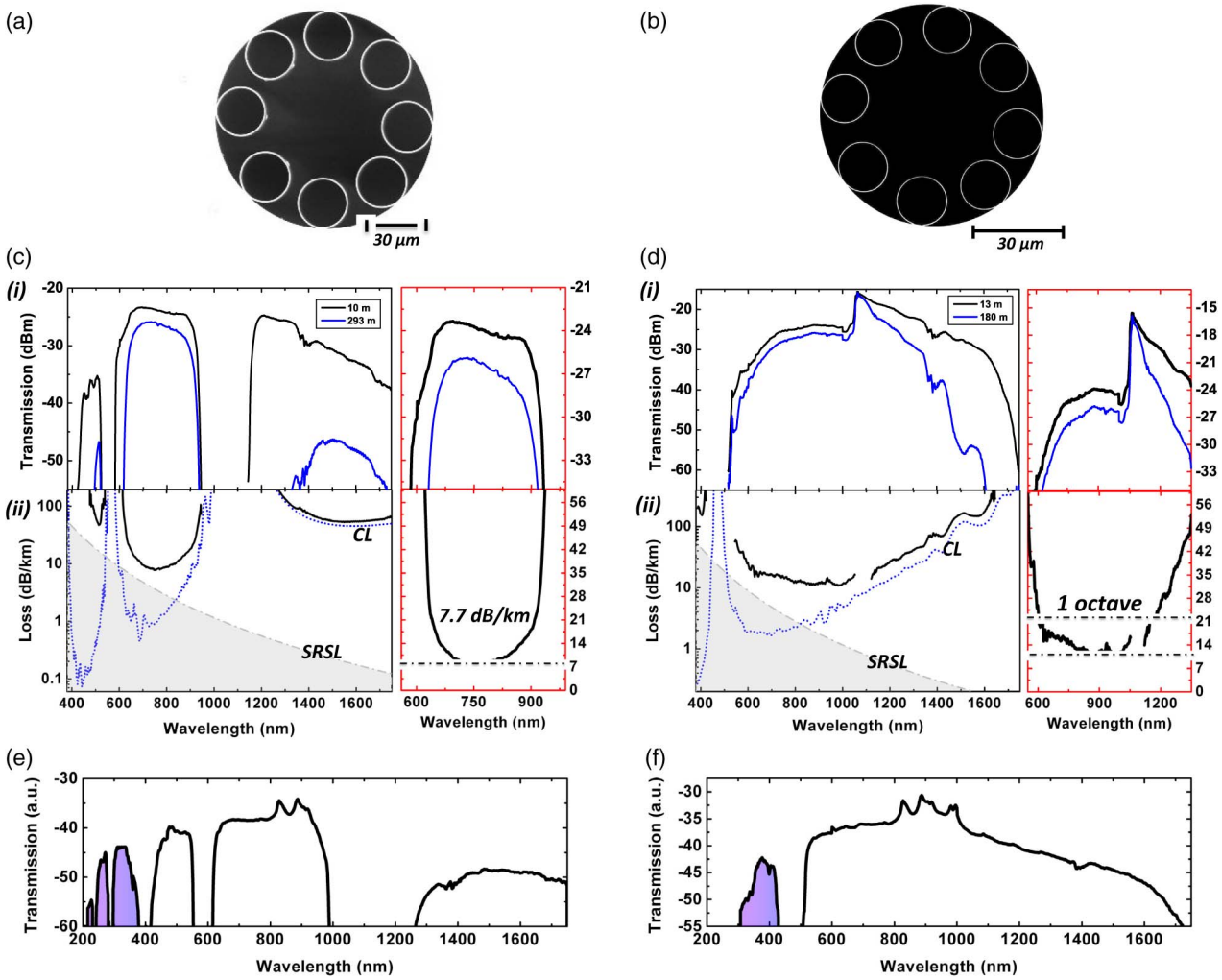

Fig. 5. SEM pictures of (a) Fiber #5 and (b) Fiber #6. Transmission curves along the two fiber pieces recorded during cut-back measurement for (c)(i) Fiber #5 and (d)(i) Fiber #6. Measured attenuation spectra (black curves) and calculated CL (dotted blue curves) for (c)(ii) Fiber #5 and (d)(ii) Fiber #6. Fiber #5 reaches a record of 7.7 dB/km, and Fiber #6 exhibits a loss in the range 10–20 dB/km over one octave [(d)(ii)]. The blanked data around 1 μm in (d)(ii) are due to the stronger supercontinuum power at 1064 nm. Bottom: Measured transmission of a 2 m long piece of (e) Fiber #5 and (f) Fiber #6, with purple-filled curve highlighting UV/DUV guidance.

<250 nm) poses fabrication challenges in keeping the circular shape of the tubes and also increases the surface scattering through larger surface roughness that results from an enhanced surface capillary wave during the draw process. Consequently, reaching the lowest loss in the shortest wavelength will be a compromise between CL (i.e., design limited) and SSL (i.e., fabrication limited). The results of this fabrication campaign are summarized in Fig. 5. The source used is a supercontinuum which consists of a piece of a nonlinear PCF and a nanosecond pulsed microchip laser providing an average spectral power around 100 mW with a stability <1%. The fiber under test was coiled into a 60 cm bend curvature and the fiber input ends were prepared using a commercial cleaver. For each transmission measurement, 10 fiber cleaves were done, demonstrating an error measurement under the resolution of the optical spectrum analyzer (Ando AQ 6315A), i.e., 0.1 dB. The white light source was coupled into the fiber using commercial coupling lenses to match the mode-field diameter between the fiber and the laser source, resulting in the present case in a coupling efficiency >90%. The figure shows the loss and transmission spectra of two fibers. The corresponding scanning electron microscopy (SEM) pictures of the fabricated fibers are shown in Figs. 5(a) and 5(b). The first one (Fiber #5) exhibits an average δ value of 2.5 μm, $t =$ 545 nm, and $R_c = 20.5$ μm. Its measured loss spectrum (cut back between 293 and 10 m long pieces) shown in Fig. 5(c)(ii) highlights ultralow loss in the first-order band with an absolute record transmission loss, for a HC-PCF of 7.7 dB/km at 750 nm. This loss figure is only about a factor of 2 larger than the silica Rayleigh scattering limit shown by the grey filled curve.

The second design (Fiber #6) presents thinner tubes ($t = 227$ nm), thus shifting the fundamental band blue edge to a wavelength as short as 515 nm [Fig. 5(d)(i)]. It exhibits an average δ value of 3 μm and $R_c = 20$ μm. An ultralarge low-loss window is demonstrated over one octave ranging from 600 to 1200 nm, with loss between 10 and 21 dB/km [Fig. 5(d)(ii)] (cut back between 180 and 13 m long pieces). This is, to our knowledge, the first time that a HC-PCF combines such a large bandwidth with such a low transmission loss. The measured transmission spectra of 2 m long sections from the two fibers are plotted in Figs. 5(e) and 5(f). Both fibers exhibit guidance in the UV domain. Remarkably, Fiber #5 shows three UV transmission bands spanning down to 220 nm (purple filling color). Reliable measurements of loss spectra for wavelengths shorter than 350 nm were prevented due to the limited dynamics of the photospectrometer.

Figures 5(c) and 5(d) also show the theoretical CL loss spectra. The CL is calculated numerically for the case of fibers with no surface roughness. Comparing $\alpha_{CL}(\lambda)$ with the measured loss shows that, for Fiber #5, the loss is dominated by the CL in the range of 1300–1750 nm, which is in the range of 80–45 dB/km. However, for the first and second higher-order bands of Fiber #5, the discrepancy between the measured loss and CL is much higher, indicative of stronger contribution of SSL. Here, the CL for a surface-roughness-free HC-PCF reaches a minimum of ~1 dB/km in the first band and ~0.1 dB/km in the second band. This trend is also observed for Fiber #6, where the CL dominates for wavelengths larger than 1000 nm, and the surface-roughness-induced SSL and CL increase become the dominant transmission loss for shorter wavelengths (typically less than 800 nm).

In addition to the just-shown low transmission loss, these fibers present a low bending sensitivity of less than 0.05 dB/turn for a 30 cm bend diameter over the whole transmission band, and reach 0.03 dB/turn at 750 nm for Fiber #5 (see Supplement 1). The modal content has also been characterized using spectral and spatial (S2) imaging techniques [34,35]. Figure 6(a) shows the typical S2 modal content and the evolution with the group delay of the interference signal Fourier transform for fiber length of $L = 5$ m and $L = 15$ m from Fiber #6. The S2 imaging system comprises an InGaAs camera and tunable laser source with a tuning range of 1010–1070 nm and minimum step size of 40 pm. At the output of the fiber, a telescope is used to collect the light recorded through the camera, which is triggered directly from the laser and controlled by a PC. For 5 m long fiber, the LP_{11} mode presents a multi-path interference (MPI) of 21.4 dB, which corresponds to a quasi-single-mode operation and increases to 22.4 dB for a length of 15 m.

The fibers' polarization-maintaining properties were explored by launching a laser beam into the fiber from a linearly polarized laser emitting at 1030 nm and a half-wave plate for polarization control. The transmitted beam is then passed through a polarizing beam splitter (PBS), and each of its two output beams is recorded by a power meter and a camera imaging its reconstructed near-field beam profile. Figure 6(b) shows the evolution of the polarization extinction ratio (PER) with the fiber length (Fiber #6 is used). The inset shows the fiber-transmitted laser power from each of the two output ports of the PBS in function with the half-wave plate angle. The deduced PER was recorded for different fiber lengths. The results show a maximum PER of 15.5 dB achieved with a fiber length of 16 m, and an evolution with the fiber length which comprises a decrease in PER as fiber length decreases for length shorter than 12 m, and then an enhancement in PER as the fiber length increases for length longer than 12 m.

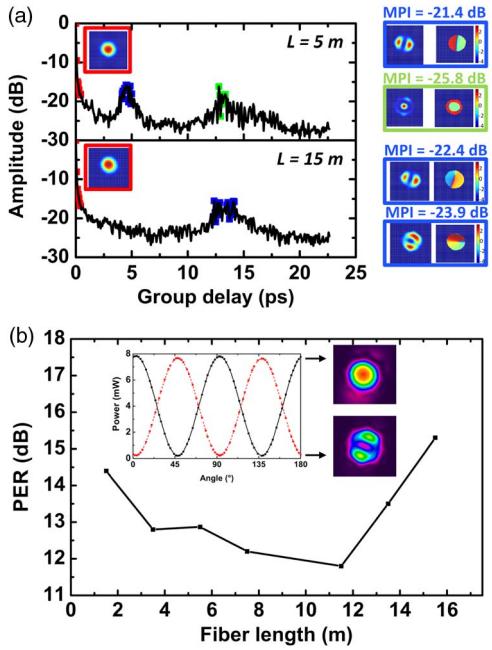

Fig. 6. (a) Group delay curves of the HOM content propagating in Fiber #6 for 5 and 15 m long pieces. The reconstructed mode field profiles are indicated with the corresponding MPI. (b) Evolution of the PER versus the fiber length.

It is noteworthy that the profiles of the crossed-polarized beams show that, for an input polarization corresponding to a maximum PER, the mode of the dominant polarization orientation is mainly that of HE_{11} while the one with the crossed polarization shows a profile of that of the LP_{11} family [inset of Fig. 6(b)]. We believe that this PER evolution with the fiber length and the fact that the mode of the crossed-polarized beams is that of LP_{11} results from the back-coupling to the core of the light scattering off the core inner surface. Indeed, by virtue of stronger optical overlap of the higher-order core modes with the core contour, the light that is coupled back from the core-surround surface is likely to couple to higher-order modes rather than the HE_{11}.

4. CONCLUSION AND DISCUSSION

In conclusion, we fabricated several SR-TL HC-PCFs guiding in the NIR–VIS–UV spectral range and showing ultraloss. The fiber cladding physical properties were adjusted for optimum confinement loss and close-to-unity modal content using the IC formalism. Among the fabricated fibers we listed, one fiber had a record loss of 7.7 dB/km at 750 nm, and a second SR-TL HC-PCF combined an octave-wide transmission band with transmission loss in the range of 10–20 dB/km. We have shown that the transmission loss is limited by CL for a wavelength longer than ~1 μm, indicating that improving the loss at these spectral ranges and with core diameters comparable to the ones reported here would require a different cladding design with stronger IC. Nested tube lattice HC-PCFs [36,37] are excellent candidates for this purpose, as their cladding modes exhibit larger azimuthal number than the reported tubular lattice for the same $n_{\mathrm{eff}} - \omega$. The challenge with such a nested tubular lattice is the difficulty in controlling the different tube thicknesses during the fabrication process and keeping them the same and constant throughout the draw. On the other hand, for shorter wavelengths (typically less than 800 nm), the fiber transmission performance is no longer limited by the fiber design but by the surface roughness. The latter affects the propagation loss of SR-TL HC-PCFs via both SSL and CL. Improving the transmission loss for a wavelength shorter than 800 nm would require reducing the surface roughness during the draw, and the cladding lattice design of any hypocycloid core-contour HC-PCF will play no significant role until the transmission loss reaches the level of 1 dB/km or below. The reported results represent an important tool in improving the loss in IC guiding HC-PCF. Given the much lower optical overlap with the core surround and the larger transverse dimensions of this type of fiber compared to PBG fibers, these results could revive the prospect of developing optical fibers with transmission loss much lower than the silica Rayleigh scattering limit if the surface roughness is reduced.

Funding. Agence Nationale de la Recherche (ANR) (Photosynth); Air Force Office of Scientific Research (AFOSR) (HOFGAS); Σ_LIM Labex Chaire, Maturation, region Limousin.

Acknowledgment. The authors thank the PLATINOM platform for help with the fiber fabrication.

See Supplement 1 for supporting content.

REFERENCES

1. T. A. Birks, P. J. Roberts, P. St.J. Russell, D. M. Atkin, and T. J. Shepherd, "Full 2-D photonic bandgaps in silica/air structures," Electron. Lett. **31**, 1941–1943 (1995).
2. F. Benabid and P. J. Roberts, "Linear and nonlinear optical properties of hollow core photonic crystal fiber," J. Mod. Opt. **58**, 87–124 (2011).
3. P. St.J. Russell, P. Holzer, W. Chang, A. Abdolvand, and J. C. Travers, "Hollow-core photonic crystal fibres for gas-based nonlinear optics," Nat. Photonics **8**, 278–286 (2014).
4. F. Couny, F. Benabid, P. J. Roberts, P. S. Light, and M. G. Raymer, "Generation and photonic guidance of multi-octave optical-frequency combs," Science **318**, 1118–1121 (2007).
5. P. Roberts, F. Couny, H. Sabert, B. Mangan, D. Williams, L. Farr, M. Mason, A. Tomlinson, T. Birks, J. Knight, and P. St.J. Russell, "Ultimate low loss of hollow-core photonic crystal fibres," Opt. Express **13**, 236–244 (2005).
6. J. von Neumann and E. Wigner, "Über merkwürdige diskrete Eigenwerte," Phys. Z. **30**, 465–467 (1929).
7. C. W. Hsu, B. Zhen, A. D. Stone, J. D. Joannopoulos, and M. Soljačić, "Bound states in the continuum," Nat. Rev. Mater. **1**, 16048 (2016).
8. F. Couny, F. Benabid, and P. S. Light, "Large-pitch Kagome-structured hollow-core photonic crystal fiber," Opt. Lett. **31**, 3574–3576 (2006).
9. Y. Wang, F. Couny, P. J. Roberts, and F. Benabid, "Low loss broadband transmission in optimized core-shape Kagome hollow-core PCF," in *Conference on Lasers and Electro-Optics* (IEEE, 2010), paper CPDB4.
10. Y. Y. Wang, N. V. Wheeler, F. Couny, P. J. Roberts, and F. Benabid, "Low loss broadband transmission in hypocycloid-core Kagome hollow-core photonic crystal fiber," Opt. Lett. **36**, 669–671 (2011).
11. B. Debord, M. Alharbi, T. Bradley, C. Fourcade-Dutin, Y. Y. Wang, L. Vincetti, F. Gérôme, and F. Benabid, "Hypocycloid-shaped hollow-core photonic crystal fiber, part I: arc curvature effect on confinement loss," Opt. Express **21**, 28597–28608 (2013).
12. B. Debord, M. Alharbi, L. Vincetti, A. Husakou, C. Fourcade-Dutin, C. Hoenninger, E. Mottay, F. Gerome, and F. Benabid, "Multi-meter fiber-delivery and pulse self-compression of milli-Joule femtosecond laser and fiber-aided laser-micromachining," Opt. Express **22**, 10735–10746 (2014).
13. A. D. Pryamikov, A. S. Biriukov, A. F. Kosolapov, V. G. Plotnichenko, S. L. Semjonov, and E. M. Dianov, "Demonstration of a waveguide regime for a silica hollow-core microstructured optical fiber with a negative curvature of the core boundary in the spectral region > 3.5 μm," Opt. Express **19**, 1441–1448 (2011).
14. F. Yu, W. J. Wadsworth, and J. C. Knight, "Low loss silica hollow core fibers for 3–4 μm spectral region," Opt. Express **20**, 11153–11158 (2012).
15. T. D. Bradley, Y. Wang, M. Alharbi, B. Debord, C. Fourcade-Dutin, B. Beaudou, F. Gerome, and F. Benabid, "Optical properties of low loss (70 dB/km) hypocycloid-core Kagome hollow core photonic crystal fiber for Rb and Cs based optical applications," J. Lightwave Technol. **31**, 2752–2755 (2013).
16. F. Benabid, F. Gerome, B. Debord, and M. Alharbi, "Kagome PC fiber goes to extremes for ultrashort-pulse lasers," Laser Focus World **50**, 29–34 (2014).
17. L. Vincetti and V. Setti, "Waveguiding mechanism in tube lattice fibers," Opt. Express **18**, 23133–23146 (2010).
18. A. N. Kolyadin, A. F. Kosolapov, A. D. Pryamikov, A. S. Biriukov, V. G. Plotnichenko, and E. M. Dianov, "Light transmission in negative curvature hollow core fiber in extremely high material loss region," Opt. Express **21**, 9514–9519 (2013).
19. M. Michieletto, J. K. Lyngsø, C. Jakobsen, J. Lægsgaard, O. Bang, and T. T. Alkeskjold, "Hollow-core fibers for high power pulse delivery," Opt. Express **24**, 7103–7119 (2016).
20. J. R. Hayes, S. R. Sandoghchi, T. D. Bradley, Z. Liu, R. Slavik, M. A. Gouveia, N. V. Wheeler, G. T. Jasion, Y. Chen, E. Numkam-Fokoua, M. N. Petrovich, D. J. Richardson, and F. Poletti, "Antiresonant hollow core fiber with octave spanning bandwidth for short haul data communications," in *Optical Fiber Communication Conference Postdeadline Papers* (Optical Society of America, 2016), paper Th5A.3.
21. H. Kawamura, "Statistics of two-dimensional amorphous lattice," Prog. Theor. Phys. **70**, 352–365 (1983).

22. M. Rechtsman, A. Szameit, F. Dreisow, M. Heinrich, R. Keil, S. Nolte, and M. Segev, "Amorphous photonic lattices: band gaps, effective mass, and suppressed transport," Phys. Rev. Lett. **106**, 193904 (2011).
23. N. M. Litchinitser, A. K. Abeeluck, C. Headley, and B. J. Eggleton, "Antiresonant reflecting photonic crystal optical waveguides," Opt. Lett. **27**, 1592–1594 (2002).
24. J. M. Pottage, D. M. Bird, T. D. Hedley, T. A. Birks, J. C. Knight, P. St.J. Russell, and P. J. Roberts, "Robust photonic band gaps for hollow core guidance in PCF made from high index glass," Opt. Express **11**, 2854–2861 (2003).
25. M. M. Z. Kharadly and J. E. Lewis, "Properties of dielectric-tube waveguides," Proc. Inst. Electr. Eng. **116**, 214–224 (1969).
26. E. A. J. Marcatili and R. A. Schmeltzer, "Hollow metallic and dielectric waveguides for long distance optical transmission and lasers," Bell Syst. Tech. J. **43**, 1783–1809 (1964).
27. M. A. Duguay, Y. Kokubun, T. L. Koch, and L. Pfeiffer, "Antiresonant reflecting optical waveguides in SiO_2-Si multilayer structures," Appl. Phys. Lett. **49**, 13–15 (1986).
28. D. Marcuse, "Investigation of coupling between a fiber and an infinite slab," J. Lightwave Technol. **7**, 122–130 (1989).
29. H. Kogelnik, "An introduction to integrated optics," IEEE Trans. Microw. Theory Tech. **23**, 2–16 (1975).
30. W.-P. Huang, "Coupled-mode theory for optical waveguides: an overview," J. Opt. Soc. Am. A **11**, 963–983 (1994).
31. L. Vincetti, "Empirical formulas for calculating loss in hollow core tube lattice fibers," Opt. Express **24**, 10313–10325 (2016).
32. F. Poletti, "Nested antiresonant nodeless hollow core fiber," Opt. Express **22**, 23807 (2014).
33. M. Alharbi, T. Bradley, B. Debord, C. Fourcade-Dutin, D. Ghosh, L. Vincetti, F. Gérôme, and F. Benabid, "Hypocycloid-shaped hollow-core photonic crystal fiber, part II: cladding effect on confinement and bend loss," Opt. Express **21**, 28609–28616 (2013).
34. J. W. Nicholson, A. D. Yablon, S. Ramachandran, and S. Ghalmi, "Spatially and spectrally resolved imaging of modal content in large-mode-area fibers," Opt. Express **16**, 7233–7243 (2008).
35. P. Calvet, "Mise en forme spatiale dans une fibre optique microstructurée pour la réalisation d'amplificateurs lasers tout fibrés pour les pilotes des lasers de puissance," Ph.D. dissertation (Université des Sciences et Technologies de Lille, 2014).
36. W. Belardi and J. C. Knight, "Hollow antiresonant fibers with reduced attenuation," Opt. Lett. **39**, 1853–1856 (2014).
37. M. S. Habib, O. Bang, and M. Bache, "Low-loss hollow-core silica fibers with adjacent nested anti-resonant tubes," Opt. Express **23**, 17394–17406 (2015).

155.185.137.52 {ts '2020-02-13 04:31:47'}